INDIUM CORPORATION
TECHNICAL PAPER

A Novel Lower-Temperature Lead-Free Solder Paste for Wafer-Level Package Application

Authored by: HongWen Zhang, Ph.D., Tyler Richmond, Jie Geng, Ph.D., and Huaguang Wang, Indium Corporation; and Tybarius Harter[1] and Diego Prado[2].

Abstract

An In-containing lower-temperature solder paste has been studied for wafer-level package (WLP) application. The daisy-chained WLP256 assemblies (SAC305 ball with 0.25mm diameter and 0.4mm pitch) were reflowed with the In-containing lower-temperature paste to form the joints under a variety of reflow profiles, whose peak temperatures ranged from 200°C up to 240°C. The paste-to-ball volume ratio was kept consistently at 1:4. The joint morphology changed with the reflow profiles. Under the 200°C peak reflow, hybrid joints were formed in which the mixing zone, dominated by the In-containing solder, was present at the PCB side while the SAC305 ball at the chip side maintained the original morphology. Increasing the reflow peak temperature above 210°C led to the SAC305 ball being fully fused with the lower-temperature solder paste and no mixing zone could be clearly identified through SEM imaging and EDX mapping. Temperature cycling reliability tests were conducted with the profile of -40°C–125°C and 20 minutes dwelling time. SAC305, reflowed with a 240°C peak temperature, was also tested as the control leg. The In-containing low-temperature solder paste performed comparable to or superior to SAC305 based on the reflow profiles being used in both drop-shock and TCT reliability. A profile peak temperature of 210°C resulted in the best TCT performance compared to the others. The crack initiation and propagation in the joints of the SAC305 ball with SAC paste occurred at the chip side. Cracking behavior in the joints of the SAC ball and lower-temperature In-containing paste maintained the similarity regardless of the reflow profiles. Additional microstructural evolution and failure analysis are still ongoing. In conclusion, In-containing lower-temperature paste can be reflowed under a relatively lower peak temperature profile (210°C peak temperature) and outperform SAC305 paste in the current WLP256 application.

Keywords: lead-free, temperature cycle, low-temperature solder, reliability, joint morphology

DR. HONGWEN ZHANG

Dr. HongWen Zhang is Manager of the R&D Alloy Group in Indium Corporation's Research & Development Department. His focus is on the development of lead-free solder materials for high temperature and/or high fatigue resistance applications, and investigating the associated technologies.

Dr. Zhang and Dr. Ning-Cheng Lee invented the mixed powder solder technique in which minor additives are used to improve the wetting and modify the bonding interface, thus increasing the bonding strength. On the basis of this technique, BiAgX® solder system was invented as an alternative high-temperature lead-free solder. Dr. Zhang is also a certified IPC Specialist for IPC-A-600 and IPC-A-610D.

email: hzhang@indium.com
Full biography:
www.indium.com/biographies

[1] *SUNY Polytechnic Institute*
[2] *Cornell University*

Introduction

The 2017 iNEMI Board and Assembly Roadmap had forecast up to a 20% adoption rate of low-temperature solder (LTS) pastes for board assembly by 2027 [1]. The major driving forces for low-temperature soldering adoption include: (1) the decrease of dynamic warpage of highly integrated packages, (2) the reduction of energy consumption during assembly, and (3) less risk for temperature-sensitive sensors.

BiSn solders, including BiSn eutectic, BiSnAg eutectic, BiSn off-eutectic, and their modifications, have been intensively investigated and considered as the leading candidates for a low-temperature soldering process. BiSn solder has a eutectic temperature of 138°C, which enables reflow at low temperatures (165–190°C peak temperature). However, the low-melting temperature limits the service temperature to a lower range as well. In addition, the intrinsic brittleness of Bi risks the drop shock reliability, especially in mobile phone and portable electronics applications.

SnIn eutectic solder exhibits a melting temperature of 118°C, which allows even lower soldering temperatures. Consequently, the service temperature would be lower as well. The SnIn system is intrinsically ductile and soft and is expected to exhibit superior mechanical shock resistance compared to the Bi-Sn system. To allow the paste to reflow at lower temperatures (i.e., 190–210°C) and maintain the remelting temperature above 180°C for higher service temperatures, DFLT paste was developed with a patented technology [3], which contains both a low-melting SnInAg solder powder and a Sn-rich solder powder in the paste. The existence of the low-melting SnIn solder in DFLT allows reflow to be feasible at a relatively low peak temperature down to 200°C or even 190°C [4]. The Sn-rich solder powders continuously dissolve into the molten SnInAg solder during reflow at lower peak temperature, shifting the joint composition towards the Sn-rich end, and finally, no low-melting SnIn eutectic phase exists in the joint after solidification. Consequently, the remelting temperature of the final joint will rise to 180°C or even higher [3]. Using a 200°C peak temperature profile, DFLT pastes had a comparable or better drop shock performance than SAC305 reflowed using the commonly used 240°C peak profile [2]. Together with the comparable TCT performance relative to SAC305, DFLT had been successfully used to stack-bond two pre-populated boards through an interposer in the soldering process with the 200°C peak temperature profile [2, 3].

The automotive industry, emerging electric vehicles, and wafer-level packages with smaller pitch sizes demand higher reliability of solder joints, namely, the elongated lifetime and/or the survival of more aggressive service conditions, than the mainstream SAC305. Currently, most of the high-reliability solders have at least four elements instead of containing only Sn, Ag, and Cu in traditional SAC, which were expected to further strengthen the solders through one or multiple of strengthening mechanisms: (1) the solution hardening, (2) the precipitate hardening, and (3) the grain/microstructure refinement, etc. In is one of the elements able to strengthen the Sn matrix through the solid solution. Also, In participates in the formation of IMC precipitates to reinforce the joint body and interfacial IMCs together with Sn to modify the bonding interface.

Previous internal reliability studies on WLP256 (SAC305 ball, 0.25mm diameter) assembly have exhibited the negative impacts on TCT reliability when using the stiff high-reliability solders. The higher strain caused by CTE mismatch between the Si chip and PCB, as well as the insufficient ductility of the stiff solder joints, were attributed to the decreased

TYLER RICHMOND

Tyler Richmond is responsible for the testing of materials targeted toward product development, as directed by the Research & Development manager in a manner that is consistent with proper testing and laboratory procedures. He is also responsible for managing and maintaining equipment and consumable lab supplies.

Tyler joined Indium Corporation in 2021 and was responsible for designing and fabricating test fixtures for mechanical and electrical assemblies using machining, metal forming, soldering, power supplies, and lab test equipment. Tyler holds a bachelor's degree in chemical engineering from Clarkson University. Tyler also completed research on silicon molecular dynamics during his undergraduate studies.

email: trichmond@indium.com
Full biography:
www.indium.com/biographies

lifetime compared to SAC305. DFLT exhibited less degradation in joint shear strength than SAC305 for chip-resistor assembly in TCT [2–4] although the DFLT joint is softer than SAC305. This led to the current attempt of using DFLT, the soft solder instead of stiff solder, to study the reliability performance on WLP256. In addition, DFLT was designed as a lower temperature solder, reflowable above 200°C. The impacts of reflow profiles (reflow peak temperature between 200–240°C) on reliability were also considered and included in the current study. The testing goal was to confirm whether DFLT could be reflowed at a temperature substantially lower than that of SAC305 but outperform SAC305 for both drop shock and TCT reliability.

Experimental

Testing Vehicles

A customized 10x10 drop shock assembly has consistently been used in the drop shock tests. Both the BGA and PCB had circular OSP pads that were 0.55mm in diameter and had a 2.54mm pitch. The size of the BGA was 50.8x50.8mm^2 and the PCB was 101.6x101.6mm^2. The thickness of BGA substrate was 1.54mm and PCB was 1.00mm-thick. The PCB design is shown in Figure 1.

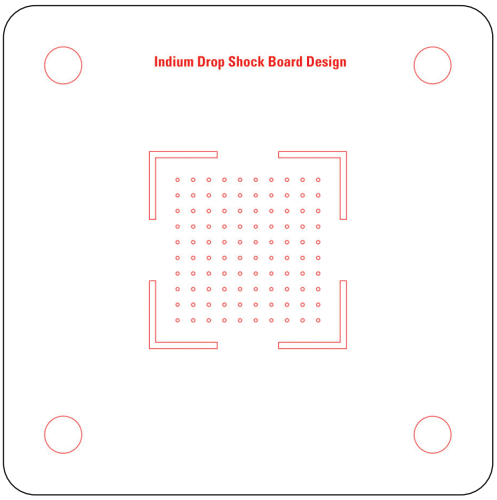

Figure 1. Indium Corporation's drop shock board design.

A daisy-chained WLP256 was used in the TCT study. The chip size of the WLP256 was 6.4x6.4mm^2, the SAC305 ball had a diameter of 0.25mm, and the pitch was 0.4mm. The PCB shown in Figure 2 had a non-solder-mask-defined (NSMD) OSP pad with a 0.3mm diameter. The PCB design allowed an electrical continuity check of each column through the rectangular pads and the electrical continuity of the entire package through the two square pads. Each assembly was connected to the data-logger for in-situ continuity monitoring.

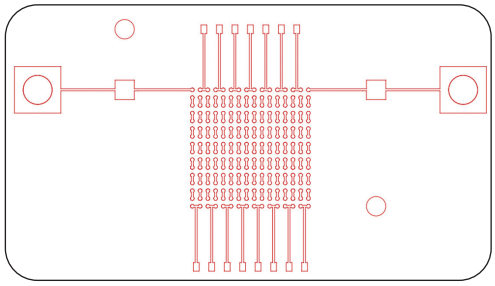

Figure 2. Daisy-chained PCB for WLP256.

Stencil Design

To build the drop shock package, SAC305 paste was printed on the BGA side with a 0.102mm-thick stencil and a circular aperture of 1.77mm in diameter. On the PCB side, paste was printed with a 0.102mm-thick stencil and a circular aperture of 0.889mm in diameter. With this stencil design, the solder alloy volume ratio between the PCB and the BGA for each joint was around 1:4 after reflow.

To build the WLP256 assembly, DFLT paste was printed onto a PCB with a 0.06mm-thick stencil and a circular aperture of 0.22mm in diameter. The paste to solder ball volume ratio was maintained consistently around 1:4, which is equivalent to the ratio of solder alloy from paste to solder ball of 1:8.

Reflow

After placing either drop shock BGA chips or WLP256 chips onto the corresponding paste-print-deposited PCBs, different profiles were tested to reflow the DFLT paste. The peak temperatures of the profiles

DR. JIE GENG

Dr. Jie Geng, Research Metallurgist, is responsible for the development of novel lead-free high-reliability solder alloys for automotive applications. Jie also investigates the assembly process technologies in electronic packaging and interconnections.

Prior to joining Indium Corporation, Jie worked as a materials scientist. In that capacity, he gained extensive experience with materials selection, design, processing, and characterization, especially as it relates to processing-structure-property relationships in various materials including ultra-high temperature alloys, lightweight alloys (Al and Mg), magnetic materials, and ceramics.

Jie received his Ph.D. in Metallurgy from the University of Surrey in the United Kingdom. He has published more than 20 journal articles in the field of materials science and engineering and also serves as a peer reviewer for numerous journals.

email: jgeng@indium.com
Full biography:
www.indium.com/biographies

used were roughly 200°C, 210°C, 220°C, and 240°C, respectively. SAC305 paste was used as the control leg, which was reflowed under a 240°C peak profile. Note that reflowing under lower peak temperatures may not fully melt SAC305 balls and form homogeneous joints with LTS paste afterwards. Figure 3 summarizes the reflow profiles used to build the testing vehicles. A plateau-type profile was used when reflowing at lower peak temperatures, in which the DFLT paste would have enough time to fully melt and merge sufficiently with a SAC305 ball. Table 1 summarizes the actual peak temperatures and the plateau times or time above liquidus (TAL >220°C).

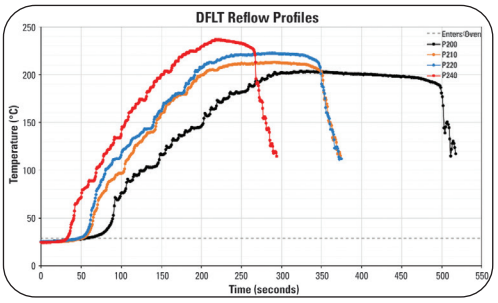

Figure 3. Reflow profiles for testing vehicles build-up.

Table 1. Features of Reflow Profiles

Profile #	Peak Temp (°C)	Plateau Time/ TAL(s)
P200	203	125s (T>200°C)
P210	213	99s (T>210°C)
P220	222	88s (T>220°C)
P240	236	84s (T>220°C)

Drop Shock Test

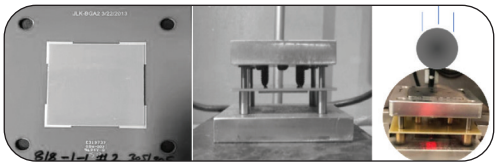

Figure 4. Ball drop test setup.

Drop shock tests were done using the customized ball-drop-tester. Figure 4 shows the testing vehicle and the ball-drop tester setup. The reflowed drop shock package was loaded onto the sample stage with the BGA chip on the bottom. A metal block was then placed on the top, with four steel pins against the board, which were at the four corners of the BGA component, as shown in the middle picture of Figure 4. A steel ball was then dropped onto the top of the metal block from a pre-determined drop height and the shock load was transferred from the four steel pins onto the board. The drop shock number was automatically counted until a BGA chip fell off the board to trigger the stop. Using the accelerometer and the strain gauge mounted on the center of board surface, the acceleration and the mechanical strain from the first drop impact (the ball would bounce up and down a few times on the board) was captured and summarized in Table 2 (drop height: 500mm; steel ball weight: 110gm). Each data point in the table was averaged from ten drops.

Table 2. Acceleration from Ball Drop Tests

Drop Height: 500mm	Ball Weight: 110gm
Acceleration (g)	6,398 ± 370
Strain (mm/mm)	-0.0038 ± 0.0002

HUAGUANG WANG

Huaguang Wang is responsible for the research and development of high-reliability, low-temperature solders in their applications. Huaguang has significant experience in the R&D environment. He was previously employed at Michigan Technological University (MTU) as a Research Assistant, where he was responsible for designing and synthesizing a novel metal/sepiolite nanocomposite for antibacterial and catalytic applications. He also evaluated the efficiency of a novel microwave heating system for materials expansion.

Huaguang recently earned his Ph.D. in materials science and engineering from Michigan Technological University, and his bachelor's and master's degrees in metallurgical engineering from Central South University.

email: huaguangw@indium.com
Full biography:
www.indium.com/biographies

Thermal Cycling Test

Daisy-chained WLP256 packages were loaded into the TCT chamber with a profile of -40°C–125°C and 20 minutes dwelling time at both the peak and valley. A data-logger was used to record the resistance change. Failure was counted when resistance increased by 100%.

Results

Drop Shock Performance

Figure 5 shows the as-reflowed joint morphology of drop shock assemblies built under different reflow conditions. Reflowed under the P200 profile, hybrid joints were achieved in which the SAC305 balls were not fully melted and merged with the DFLT paste during reflow. A mixing zone is observed on top of the PCB pad featured with a different contrast in Figure 5A. When reflowed at P210 and above, the mixing zone was not visible from the optical image, as shown in Figure 5B. With higher reflow temperatures above P220, the joints, similar to SAC305 P240, were prone to become elliptical shapes, which indicated the SAC ball and DFLT paste were fully merged during reflow.

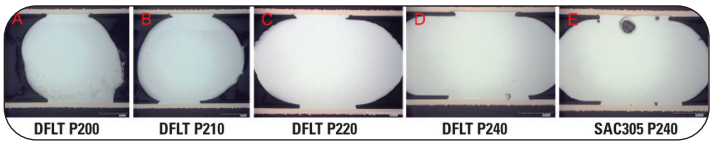

Figure 5. Joint morphology of as-reflowed drop shock assembly.

SEM images and the associated EDX mapping as seen in Figure 6 have selectively shown the time-zero joint microstructure of DFLT drop shock packages reflowed under P200 and P220 profiles, respectively. The hybrid joint structure is clearly identified for the P200 reflow. The top circular area of the joint was dominated by SAC305, which is In-free and is darker than the remaining area (the mixing area) shown in Figure 6D; In-indexed EDX mapping shows the distribution of In. Ag3Sn particles inside this top circular area maintained the typical dendrite structure as shown in Figure 6E. The mixing area is brighter than the top dark circular area shown in Figure 6D, indicating the existence of In. The mixing area was formed after merging the molten DFLT paste and the partially dissolved SAC305 ball during reflow. Inside the mixing area, two In-containing phases, including both the bright In-rich phase and the not as bright In-containing Sn-rich phase shown in Figure 6D, are clearly seen. Ag-containing particles inside the mixing zone are scattered along (1) the boundary between In-rich and In-containing Sn-rich phases and (2) interfacial IMCs above PCB Cu pad. The joint from the P220 reflow, Figure 6F–J, no longer exhibited the mixing zone. However, well-dispersed Ag dendrites are visible in the entire joint as shown in Figure 6J. In is associated with the formation of the solid solution Sn matrix and the Ag dendrites.

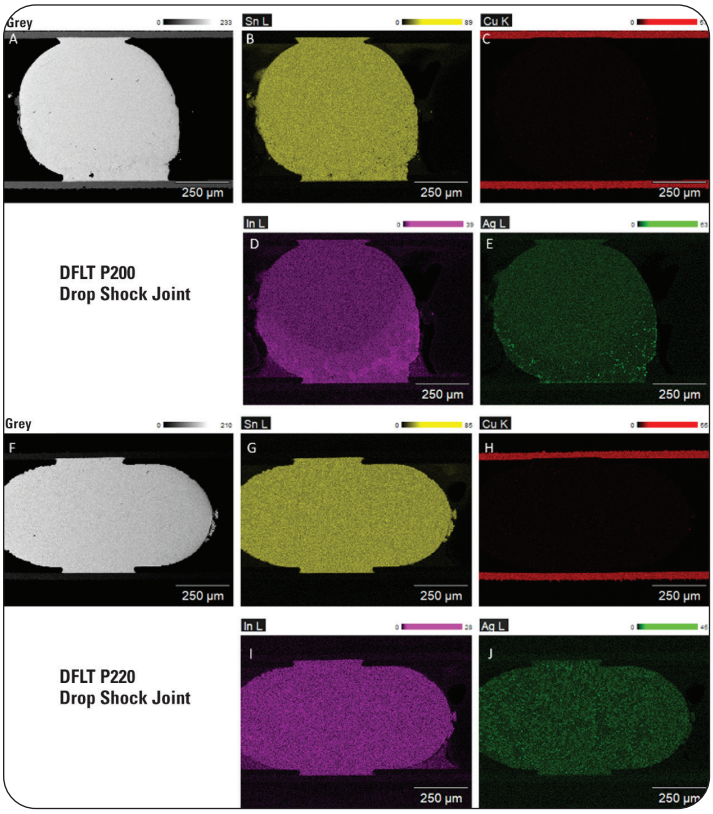

Figure 6. Joint morphology of DFLT drop shock boards reflowed with P200 (A–E) and P220 (F–J) profiles.

Figure 7 shows the joint microstructure under higher magnification and the associated EDX mapping indexed with Ag and In right above the PCB pad. In-rich, In-containing Sn-rich, and In-free areas were clearly present in the In-indexed EDX image of the P200-reflowed joint, as labeled in Figure 7C. Inside the In-free area, the SAC305 ball maintained the original microstructure featured with Ag3Sn-dendrites in the Sn matrix. In addition to both In-rich areas and Sn-rich areas inside the mixing zone, In was also involved with the Ag-containing IMC particle formation, which was confirmed by overlapping both Ag-indexed (Figure 7B) and In-indexed mapping images (Figure 7C). These particles were seen to be scattered either at the boundary between the In-rich phase and in the In-containing Sn-rich phase, or right on top of interfacial IMC layer. The IMC particles were composed of Ag, Sn, and In. However, the In-rich area was not detected when reflowed under both P220 and P240 profiles (Figure 7D–I). Both joints showed the typical dendrite structure, similar to the common SAC305 joint, although the P240 reflow seems give a finer interspacing between the dendrite arms (Figure 7H) than P220 (Figure 7E). The P220 profile (Figure 7E and F) had some scattered coarse IMC particles (Ag/In/Sn, brighter dots) among the dendrite arms while the P240 profile seldom showed the scattered coarse IMC particles (Figure 7H and I).

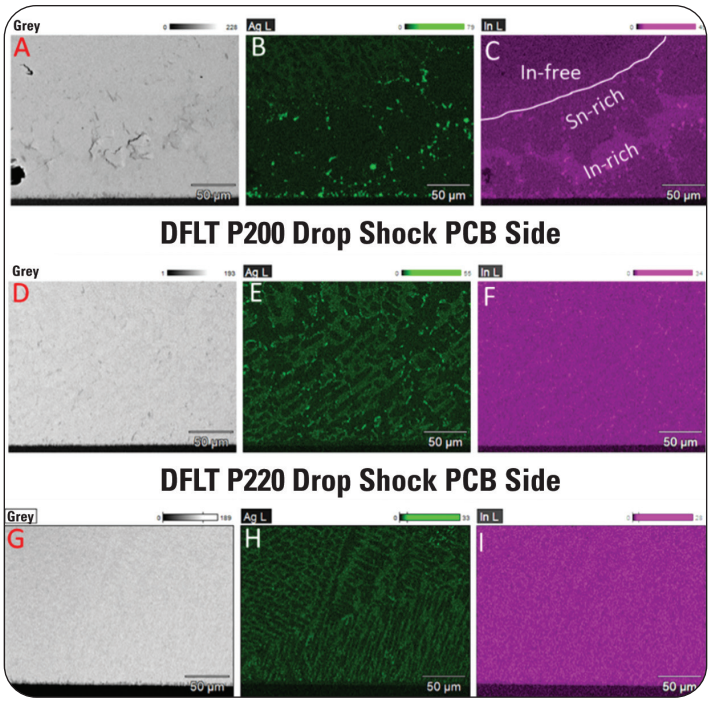

Figure 7. The enlarged joint microstructure and EDX mapping at the area on the PCB pad.

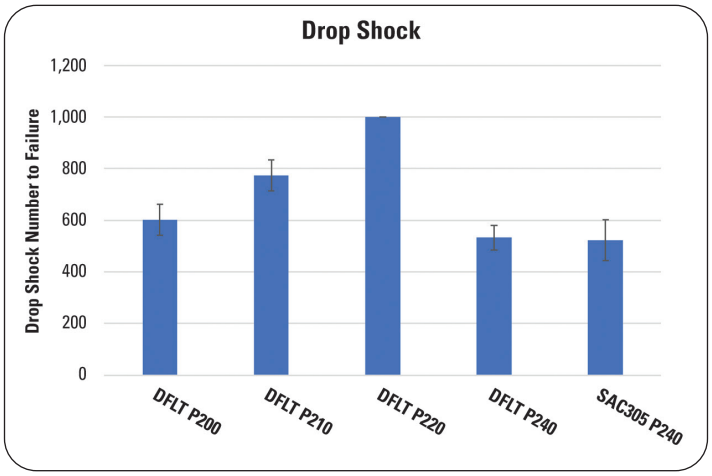

Figure 8. Impacts of reflow profiles on drop shock performance.

The reflow profiles indeed impact the drop shock performance. Figure 8 shows the drop shock number to failure for both DFLT and SAC305. Table 3 has summarized the average drop shock number to failure and the improvement over SAC305. First, regardless the profiles, DFLT always outperformed SAC305. When reflowed at P220, DFLT had the best drop shock performance, where no BGA chips fell off the PCB, even when reaching 999 drops (the test limits and the test automatically stopped afterwards). It had more than 91% improvement over SAC305. The P210 profile led to around 50% improvement of drop shock performance. When reflowed under the same 240°C profile, SAC305 and DFLT had almost identical drop shock performances.

Table 3. Summary of Drop Shock Performance

ID	Drop Shock Performance		Improvement over SAC305
	Avg. # of Drops to Failure	Error	
SAC305 P240	523	79	0
DFLT P200	602	61	15.1%
DFLT P210	774	60	48.0%
DFLT P220*	>999	0	>91.0%
DFLT P240	533	47	1.91%

All drop shock failures ruptured at the PCB side and exposed the surface right above the PCB pad. Figure 9 shows the rupture surface after drop shock failure. Since DFLT P220 did not fail, even after reaching the tester limit, no drop shock rupture was captured. DFLT P200 (Figure 9A–C) and DFLT P210 (Figure 9D–F) had particles/debris on the rupture surface while DFLT P240 (Figure 9G–I) and SAC305 (Figure 9J–L) had flakes on the surface.

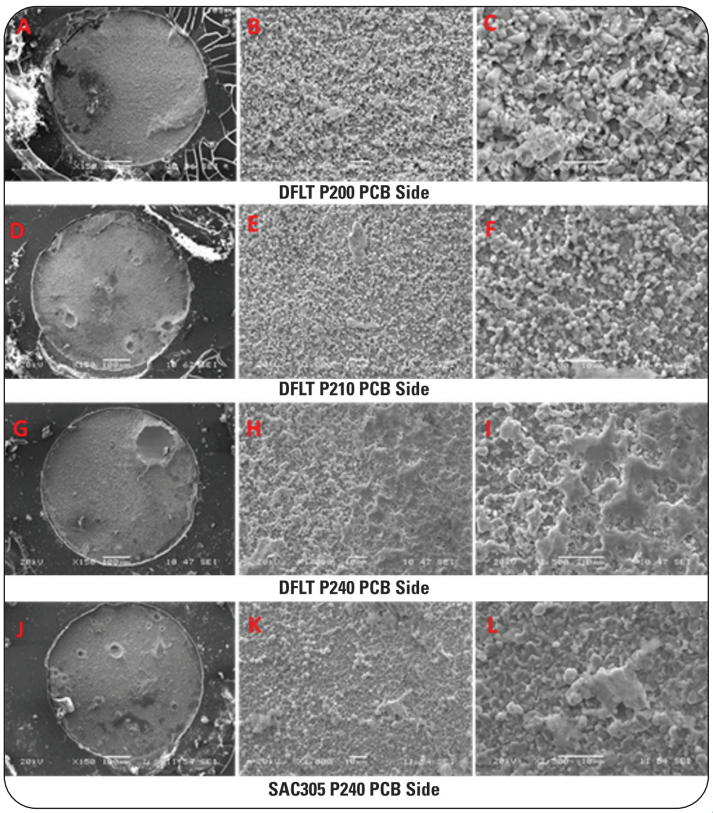

Figure 9. Rupture surface of drop shock failed packages at the PCB side.

Table 4. EDX Analysis of Drop Shock Rupture Surface

Wt%	PCB Side				Chip Side			
	Sn	In	Ag	Cu	Sn	In	Ag	Cu
SAC P240	40.46		0.21	59.62	70.6		0.44	26.97
DFLT P200	47.18	10.95	0.43	41.44	62.7	10.74	4.32	22.24
DFLT P210	41.26	4.2		54.54	67.8	6.44	4.14	21.62
DFLT P240	51.27	8.93		39.80	65.53	2.09	0.52	31.85

Table 4 summarizes the composition of the mirrored rupture surfaces from both the PCB and chip sides using EDX analysis. The significant amount of Cu on the rupture surfaces at both ends indicated that the drop shock failure was mostly inside the interfacial IMC layer. DFLT also had In detected on the rupture surfaces, which indicated the involvement of In on interfacial IMC formation. In (atomic number 49) and Sn (atomic number 50) are neighbors in the periodic table, having similar chemical reactivity based on the similar atomic radius (In:1.56Å and Sn:1.45Å) and similar electronegativity (In:1.78 and Sn:1.96). The In-Cu binary phase diagram also confirmed the formation of various CuIn IMCs. Thus, it is reasonable to speculate that In may form $Cu_6(SnIn)_5$ or $Cu_{11}(SnIn)_9$ or even a mixture of both. It is still unclear which way is dominant and additional investigation is still ongoing.

Thermal Cycling Tests

Figure 10 shows the joint morphology of WLP256 assemblies. The optical images barely tell the existence of the mixing zone, although DFLT P200 shows a slightly non-spherical joint shape. Increasing the peak temperature leads to the spherical joint. For lower temperature soldering, the SAC305 ball may not fully melt and form the spherical solder joint well with low-temperature solder paste. To achieve the optimized solder joint, both the paste volume relative to solder ball and the reflow peak temperature impact the joint morphology and the associated reliability.

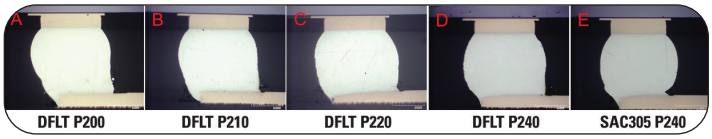

Figure 10. Joint morphology of as-reflowed WLP256 assembly.

Figure 11A-E shows the existence of the mixing zone right above the PCB pad for the DFLT P200 joint. Different from the drop shock joint, the In-rich phase is barely seen in the mixing zone and visually In forms the IMC precipitates together with Ag (Figure 11D–E). With the drop shock assembly joints reflowed at 200°C, both In-rich and Sn-rich phases are seen. However, it is difficult to tell both phases in WLP joints from EDX mapping in Figure 11D and E. The

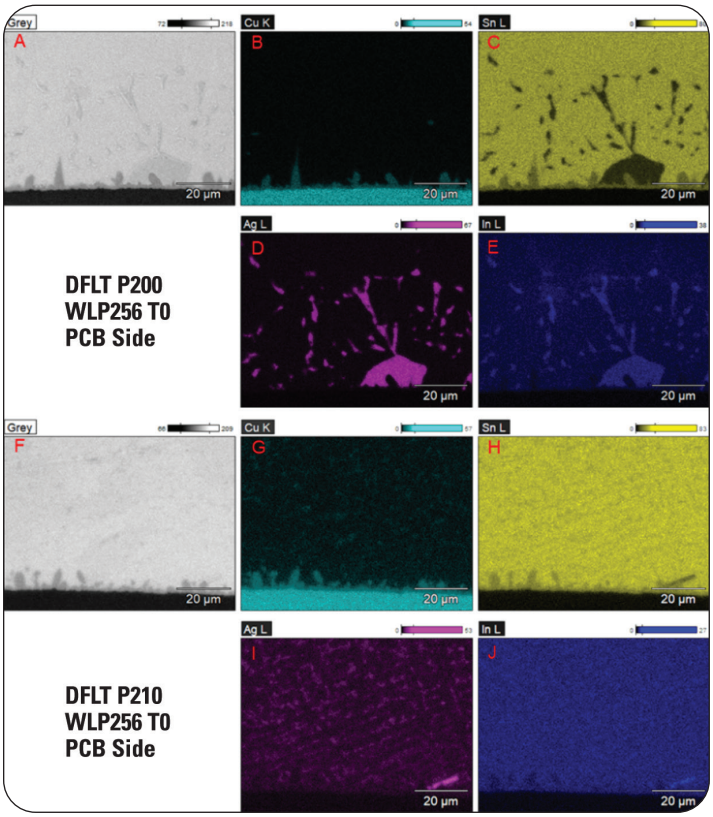

Figure 11. Joint morphology of DFLT at the PCB side reflowed under P200 (A–E) and P210 (F–J).

different solder paste volume to SAC ball ratio of WLP256 compared to the drop shock package was attributed to the change of the joint morphology.

P210 reflow led to the formation of the homogeneous joint, and the mixing zone was not able to be seen. Also, In reacted with Ag to form the IMC precipitates and resulted in the dendrite structure of the entire joint shown in Figure 11 I and J. In had also been detected in the joint matrix, indicating the formation of the In and Sn solid solution. Similar joint morphology was found for all DFLT joints reflowed above the 210°C peak temperature. The microstructure of SAC305 joints were visually similar to that of DFLT reflowed 210°C and above.

WLP256 packages were tested with a -40°C/125°C and 20min dwelling time TCT profile. The Weibull plot in Figure 12 summarized the characteristic life and the slope of both DFLT and SAC305. The data was reorganized in Table 5. Regardless of the reflow profiles, DFLT enhanced the characteristic life by at least 10% compared to SAC305. Under the same P240 profile, DFLT showed more than 15% improvement. DFLT P210 showed the best performance with the characteristic life of 824.5 cycles, which is more than 30% better than SAC305.

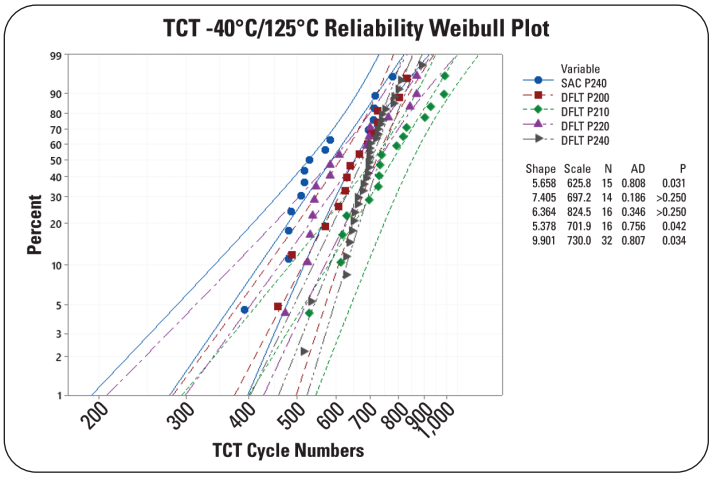

Figure 12. Impacts of reflow profiles on TCT performance.

Table 5. Summary of TCT Performance

ID	Characteristic Life (cycles)	Improvement over SAC305	Slope
SAC305 P240	625.8	0	5.658
DFLT P200	697.2	11.41%	7.405
DFLT P210	824.5	31.75%	6.364
DFLT P220	701.9	12.16%	5.378
DFLT P240	730.9	16.79%	9.901

Discussion

DFLT outperformed SAC305 in both drop shock and WLP256 TCT, regardless of the reflow profiles. Reflow peak temperatures between 210–220°C resulted in the best performance among all profiles—more than 90% improvement in drop shock performance and 30% enhancement in TCT compared to SAC305 P240. Further increasing and decreasing the reflow peak temperature reduced the performance. Normally, the impacts of the reflow profile on reliability for DFLT could be rationalized from the associated joint microstructure and the microstructural evolution.

In terms of drop shock performance, along with the joint body morphology, the interfacial IMC would be another main contributor towards the performance since all the failures were along the interface between solder and PCB pad. Commonly, IMC thickness changes with the reflow profiles. In Figure 13, DFLT P220 showed the thinnest interfacial IMC layer, and DFLT P200 had the thickest IMC layer, while DFLT P240 was in-between the two. The best drop shock performance of DFLT P220 could be attributed to the thinnest IMC thickness; however, the thickest IMC layer of DFLT P200 did not make it perform the worst. Instead, DFLT P240 performed the worst. Possibly, the mixing zone at the PCB side from P200 may absorb more shock energy in drop shock since it is softer and easier to deform. More investigation is ongoing.

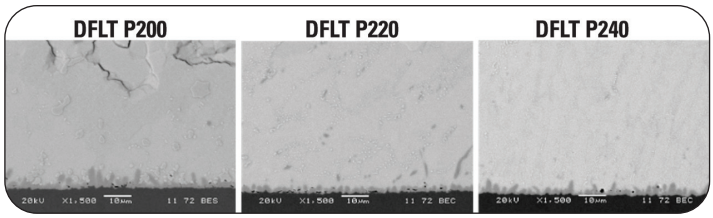

Figure 13. Interfacial IMC morphology at the PCB side with different reflow profiles.

After 1,000 cycles of TCT, the WLP256 assemblies were taken out of the chamber for failure analysis. The assembly was cross-sectioned along the outmost row or column. Figure 14 (see next page) summarizes the joint morphology (optical images) of all 16 joints along the outer-most row/column for DFLT P200, DFLT P210, and SAC P240. The corner joints were the ones that had the most severe cracking (#1 and #16 are the corner joints). Most of the cracks were formed inside the solder at the WLP256 chip side. Under the same conditions, SAC305 P240 had 11 out of 16 joints that showed full cracks at the chip side and the remaining ones had partial cracks; these are summarized in Table 6. DFLT had fewer numbers of joints having full cracks and the partial cracking close to chip was commonly seen in the joints. Occasionally, the partial cracking was observed at the PCB side for both DFLT and SAC305 joints. It was also noticed that in some cases PCB Cu pads were slightly lifted after TCT, which indicated the damage in the PCB laminate.

Table 6. Cracking Length After TCT for WLP256

ID	<25%	25~50%	50~75%	75~100%
SAC305 P240	4	1	0	11
DFLT P200	9	2	1	4
DFLT P210	11	2	3	0
DFLT P240	9	3	2	2

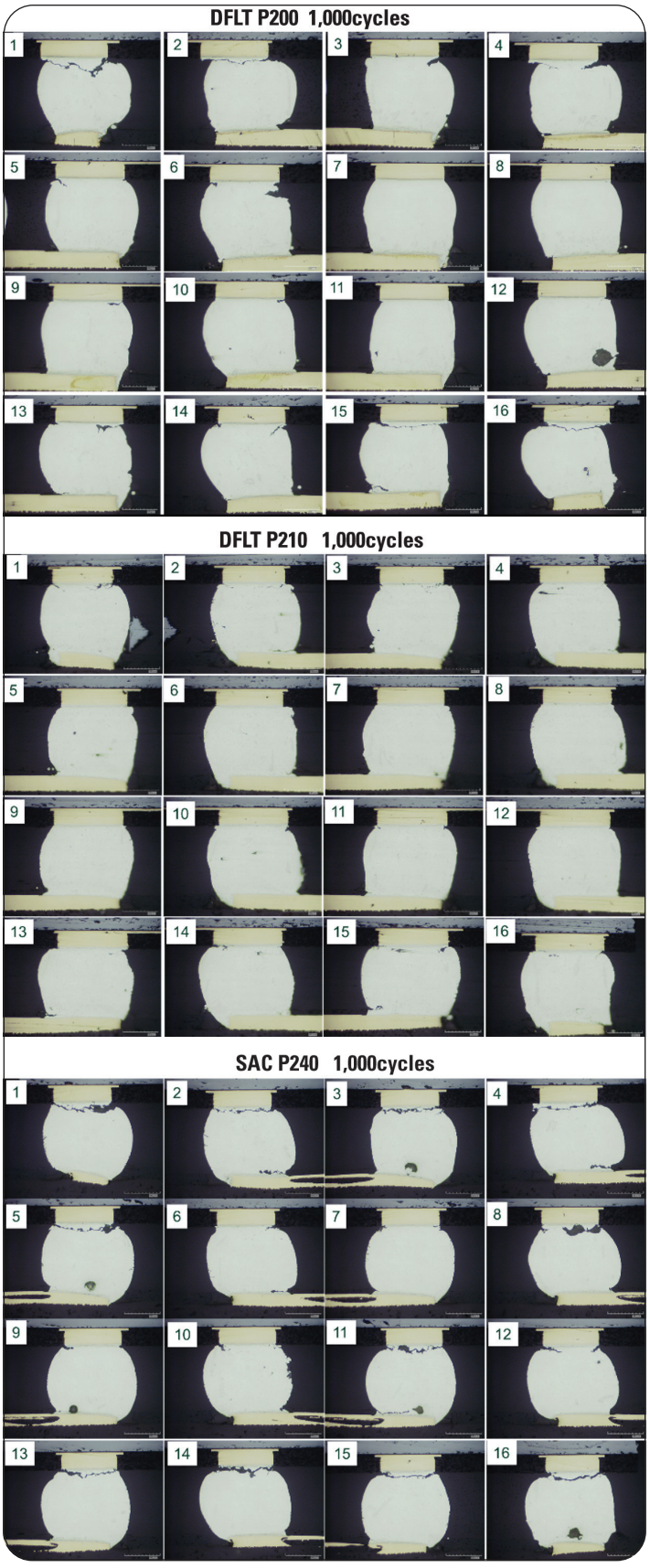

Figure 14. Joint morphology of WLP256 assembly after 1,000 cycles of TCT.

Figure 15 shows the SEM images and EDX mapping of selected corner joints after 1,000 cycles of TCT, which had cracks close to the WLP chip. The strain/stress caused by the CTE mismatch was concentrated at the interface between the Si wafer and solder (Si, CTE=2~4ppm and solder CTE=27ppm); this was in line with the cracks seen at the WLP chip side. Coarse and scattered IMC particles (Ag/In/Sn) were seen near the cracked area while the area far from the cracks maintained the original dendrite structure. The center joints in the outer-most row/column had only small corner cracks or no cracks at the WLP chip side, as shown in Figure 16 (see next page). Also, only limited numbers of bright particles were seen at the joint corners (Figure 16B, E, and H). The dendrite structure clearly dominated the entire joints of SAC305, P240, and DFLT P210. DFLT P200 still maintained the mixing zone on the PCB side and the dendrite structure inside the top of the SAC305 ball.

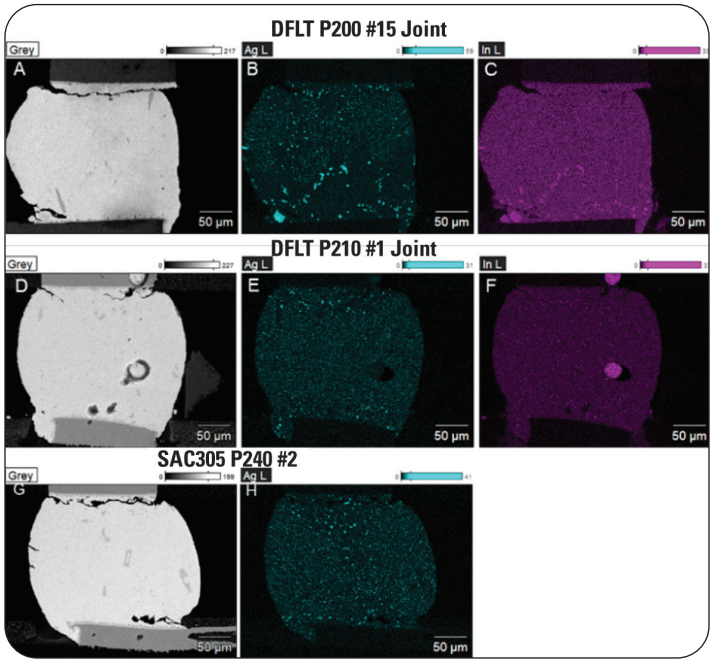

Figure 15. Selected corner joint morphology of WLP256 assembly after 1,000 cycles of TCT.

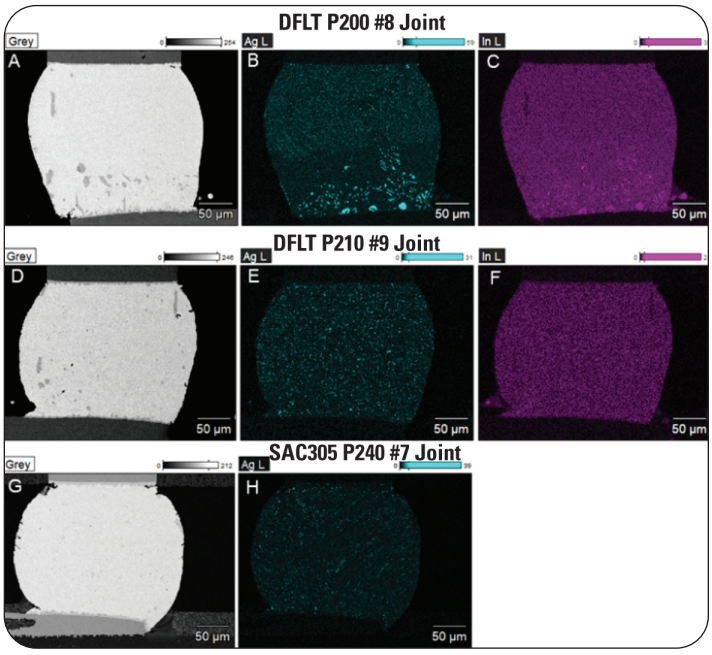

Figure 16. Selected center joint morphology of WLP256 assembly after 1,000 cycles of TCT.

The joint morphology indeed changed with different reflow profiles. The lower peak temperature (P200) resulted in the formation of the hybrid joints where the mixing zone existed beneath the BGA balls. The hybrid joints still outperformed SAC305 in both drop shock testing and TCT, although they did not perform the best among all profiles. The traditional P240 SAC profile did not make DFLT perform the best either. Instead, DFLT P210 and DFLT P220 had the best TCT and drop shock performance, which might have allowed the formation of the homogeneous joints. The failure modes remain the same for both DFLT and SAC305, regardless of the reflow profiles and the associated joint microstructure. In was observed to participate the formation of interfacial IMCs, the Ag-containing IMC precipitates, and the SnIn solid solution. Although In is assumed to be the contributor of the improved performance, the underlying mechanism is still an ongoing investigation.

Conclusion

DFLT was demonstrated to outperform SAC305 in both drop shock testing and WLP256 TCT regardless of the reflow profiles. Reflow profiles impacts on the performance were observed, in which P210 and P220 (the lower reflow peak temperature) had the best performance with both TCT and drop shock testing among all profiles. Hybrid joints were seen for the P200 reflow profile while the higher reflow temperatures led to the formation of the homogeneous joints. It was noticed that the hybrid joints did not underperform the homogeneous joints when reflowed using the traditional SAC profile. The failure modes of DFLT for all profiles were the same as SAC305. In was involved in the formation of the interfacial IMC, the Ag-containing IMC precipitates, and the solid solution matrix. In is assumed to be the main contributor towards the improved performance, although more insight studies are still ongoing.

Acknowledgment

The authors would like to thank their colleagues from Indium Corporation: Yan Liu, Christine LaBarbera, Christopher Nash, Jonas Sigfrid, Claire Hotvedt, and Fiona Chen for their support in this project. The authors would also like to acknowledge Jingya Huang and Anne Bazan for their assistance in reviewing this paper.

References

1. HongWen Zhang, et al., "An Alternative Lead-Free Low-Temperature Solder with Excellent Drop Shock Resistance," Proceedings of SMTA International, 2020, pp. 280–290.
2. Haley Fu, et al., "iNEMI BiSn-Based Low-Temperature Soldering Process and Reliability Project Report," iNEMI Low-Temperature Soldering Workshop, April 24, 2019.
3. HongWen Zhang, et al., "Low-Temperature Melting and Mid-Temperature Melting Lead-Free Solder Paste with Mixed Solder Alloy Powders," Patent application, US 2020/0353572 A1.
4. Baker, H., et al., (1990). ASM Handbook, Volume 3: Alloy Phase Diagram, 2.260, ASM International.
5. HongWen Zhang, et al., "A Novel Lead-Free Low-Temperature Solder with Excellent Drop Shock Resistance," Proceeding of International Microsystems, Packaging, Assembly and Circuits Technology Conference (IMPACT) 2021, pp. 224–230.
6. HongWen Zhang, et al., "Lead-Free, Low-Temperature Solder Paste for Drop Shock Critical Applications," Proceeding of APEX IPC Expo 2022, S20.